Journal of the Mechanics and Physics of Solids 62 (2014) 194–208

Contents lists available at ScienceDirect

Journal of the Mechanics and Physics of Solids

journal homepage: www.elsevier.com/locate/jmps

Mitigating impact/blast energy via a novel nanofluidic energy capture mechanism

Baoxing Xu [a], Yu Qiao [b,c], Xi Chen [a,d,e,*]

[a] *Columbia Nanomechanics Research Center, Department of Earth and Environmental Engineering, Columbia University, New York, NY 10027, USA*
[b] *Program of Materials Science & Engineering, University of California – San Diego, La Jolla, CA 92093, USA*
[c] *Department of Structural Engineering, University of California – San Diego, La Jolla, CA 92093-0085, USA*
[d] *International Center for Applied Mechanics, SV Lab, School of Aerospace, Xi'an Jiaotong University, Xi'an 710049, China*
[e] *Department of Civil & Environmental Engineering, Hanyang University, Seoul 133-791, Korea*

ARTICLE INFO

Article history:
Received 5 March 2013
Received in revised form
16 August 2013
Accepted 28 September 2013
Available online 11 October 2013

Keywords:
Energy capture
Impacting wave
Nanoconfined liquids

ABSTRACT

To effectively mitigating intense impact and blast waves, a novel protection mechanism is proposed in this study where a significant amount of the incident energy can be temporarily captured as potential energy in a nonwetting liquid-nanoporous material system, thereby weakening the peak pressure and elongating the impact pulse. When the pressure of a compressive wave traveling in a liquid overcomes the capillary resistance, the liquid molecules quickly intrude into nanopores while retaining highly compressed form. The incident energy is thus captured (temporarily stored) in nanopores in the form of potential energy of intercalated water molecules, and then gradually released upon unloading (which makes the system reusable). Comparing with other energy absorption materials, the present system has the unique advantage of low activation pressure and high energy density. Using comprehensive molecular dynamics (MD) simulations, the effects of several key parameters (e.g., impact velocity, nanopore size, and pore composition) on energy capture are investigated, and the molecular mechanism is elucidated. The findings are qualitatively validated by a parallel blast experiment on a zeolite/water system.

1. Introduction

Conventional energy absorption materials, such as foams and honeycombs, dissipate energy through cell buckling and extensive plastic deformation (Gibson and Ashby, 1997). Recent improvements, including material selection and cell geometry optimization, are toward the goal of enhancing their capabilities for mitigating blast or impacting waves (Cao et al., 2005; Evans et al., 2001; Nemat-Nasser et al., 2007; Schaedler et al., 2011). For instance, Hutchinson et al. (Dharmasena et al., 2008; Xue and Hutchinson, 2004) studied the buckling mechanism of sandwich plates of different cell structures. Tilbrook et al. (2006) developed an analytical model to elucidate the impulsive response of sandwich beams, and found that an overlap in time scale could enhance shock resistance. Evans et al. (2010) proposed that the energy absorption capability can be enhanced by using a hollow micro-lattice. Nevertheless, upon a high-speed impact loading or blast wave,

---

[*] Corresponding author at: Columbia University, Department of Earth and Environmental Engineering, Columbia Nanomechanics Research Center, 500 West 120th Street, New York, NY 10027, United States. Tel.: +1 212 854 3787; fax: +1 212 854 6267.
E-mail address: xichen@columbia.edu (X. Chen).

0022-5096/$ - see front matter Published by Elsevier Ltd.
http://dx.doi.org/10.1016/j.jmps.2013.09.022

due to the short timeframe and highly localized damage (e.g., shear localization and local softening), the failure stress may be quite low (Zhu et al., 1997) which significantly reduces the overall protection capacity (Côté et al., 2004; Radford et al., 2007), the system response may be quite slow and insufficient for blast/impact mitigation (Lindberg and Florence, 1987; Moss et al., 2009), and the material may not be used repeatedly after cell buckling or fracture.

Recently, nanoporous materials became attractive for high-performance energy dissipation (Lee et al., 2010; Misra et al., 2008; Teo et al., 2007), in part because the nano-sized cells are smaller than shear band (thus cell collapse and condensation would provide a local hardening mechanism, instead of local softening) and have faster response time. Han et al. (2008) found that the energy dissipation density of a nanoporous silica was on the order of 300 J/g. Kazemi-Kamyab et al. (2011) carried out impact experiments on nanoporous aluminum with various porosities, and argued that that the energy absorption and stress attenuation performances depend on the porosity, pore structure, as well as the interaction between pore gas flow and solid wall. Moreover, when nanoporous materials are immersed in a non-wetting liquid, the pressure-induced infiltration process can convert part of the external mechanical work to the excessive solid–liquid interfacial tension, further enhancing energy absorption (with an energy density that exceeds 100 J/g) (Eroshenko et al., 2001; Han and Qiao, 2006; Zhao et al., 2009b). The process is reversible (such that the system may be used repeatedly), and the liquid phase helps to reduce localized damage, which achieves high energy density (Chen et al., 2006; Qiao et al., 2007).

A major dilemma of all preceding energy absorption or dissipation mechanisms is the intrinsic conflict between the required high energy density (on mass or volumetric basis) and the desired low working pressure (for safety and comfort). That is, the total absorbed energy can be estimated (on the zero order) as $E=PV$, where P is the pressure under which the energy mitigation mechanism works (e.g., for buckling, plastic deformation, or liquid infiltration) and V is the associated system volume reduction. To achieve a high energy density (E per mass or volume), P must be as high as possible; but such a system becomes “hard”, not only uncomfortable, but also unsafe if P exceeds the safety threshold of the personnel/devices to be protected (the pressure of the transmitted wave can never be lower than the working pressure, P). In order to solve this dilemma, novel energy mitigation mechanism that has at least one more degree of freedom needs to be discovered.

In this paper, we report a novel nanofluidic energy capture (NEC) mechanism through which an intensive impact or blast energy can be effectively mitigated. This mechanism is underpinned by the unique characteristics of nanopores such that, upon a pressure wave loading, a non-wetting liquid phase can infiltrate into the nanopores to reduce the overall system volume, and the small ligament length and large impedance mismatch enables the energy capture effect, where a significant portion of the incoming kinetic energy is temporarily captured as the potential energy of invaded liquid molecules in nanopores. Furthermore, the ultralarge surface area and nanoscale confinement helps to “lock” the wave energy in nanopores temporarily, significantly weakening the incoming energy, lessening peak pressure, elongating impact pulse, and leading to an unprecedented performance of impact/blast energy mitigation (which is also reusable).

2. Description of NEC mechanism

The liquid–solid interfacial interaction is prominent at the nanoscale (Falk et al., 2010; Joseph and Aluru, 2008; Sparreboom et al., 2009; Xu and Chen, 2013), which enables many unique nanofluidic behaviors (e.g., enhanced transport (Holt et al., 2006; Hummer et al., 2001), strong size-dependence (Pascal et al., 2011)) and underpins novel devices such as the nanofluidic thermal machine (Xu et al., 2011b), pump (Liu and Li, 2010), and energy harvester (Heyden et al., 2007), among others. However, the intriguing nanofluidic intercalation behavior upon strong dynamic loading remains less explored.

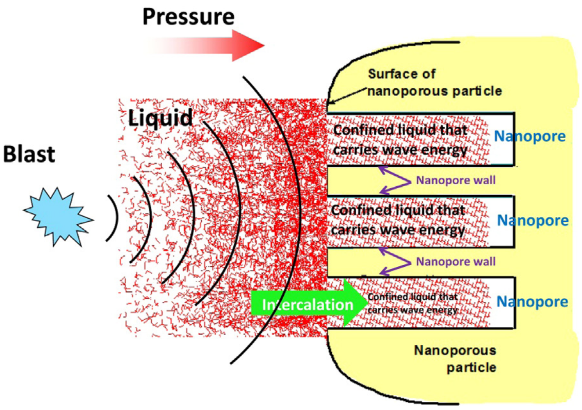

Fig.1. Schematic of the nanofluidic energy capture (NEC) mechanism. Upon a blast or impact stress wave, the solvent molecules and solvated ions become highly compacted as they intercalate into the nanopores. The invaded molecules/ions rearrange themselves in a relatively ordered configuration while retaining high wave/potential energy. Within a short time frame, a large amount of impact/blast energy can be transferred into the potential energy of the confined liquid and temporarily trapped inside the nanopores, leading to a substantial mitigation of the impact/blast stress wave.

With reference to the schematic Fig. 1, a nanoporous material is immersed in a non-wetting liquid and the pores are initially empty. As an external wave pressure is applied on the system, when the pressure exceeds a threshold (P_i), the liquid molecules/ions can overcome the capillary resistance and rapidly infiltrate into the nanopores. The intercalated liquid phase carries the wave energy, and unlike in large pores, the confined energy may not transmit out through the nanopore walls and is effectively "captured" inside in the form of potential energy of the invaded molecules. This "nanofluidic energy capture" (NEC) effect should be attributed to the nearly incompressible nanopore walls and the large impedance mismatch across the solid–liquid interface. The characteristic time of the pressure induced infiltration is around nanosecond, which also ensures a fast response of the system with respect to intense stress wave loading. Upon unloading, the confined liquid diffuses out of nanopores (at a much slower rate as compared to the infiltration rate) so that the captured energy is released slowly. Thus, the process not only significantly reduces the peak load, but also elongates the impulse duration, and the system is fully reusable. This mechanism is therefore distinct from the impulse confinement phenomenon observed in granular materials (Daraio et al., 2006; Hong, 2005).

The "captured" energy in the NEC process can be estimated as $E=P_wV_p$, where P_w is the wave pressure and V_p is the nanopore volume (typically 40–80% in nanoporous materials). Thus, the more intense the wave is (i.e., the higher the P_w is), the higher the wave mitigation efficiency would be. Meanwhile, the NEC activation/working pressure (P_i), i.e., the pressure at which the liquid intercalation takes place, is determined by the capillary effect (effective surface and interface energies) and is independent of P_w. That is, such a NEC system can capture high-pressure (P_w) wave energy at a low threshold pressure (P_i), attractive to mitigating intense stress waves while ensuring safety and comfort of protected devices/personnel. In what follows, atomistic simulations and experiments are carried out to quantitatively understand the NEC mechanism.

3. Atomistic simulation of NEC and molecular mechanism

3.1. Model and the computational method

Fig. 2 shows the computational cell which is developed on the basis of Fig. 1. A carbon nanotube (CNT) is employed to model a smooth nanopore structure with length of L_0 and diameter of D. Its left end is open and immersed in a water reservoir; its right end is closed by a rigid carbon plane to quantify the length of CNT. The initial density of water inside the reservoir is close to that of bulk water, $\rho_0=998.0\,\mathrm{kg/m^3}$ at one atmosphere pressure (1 atm) and 300 K. The reservoir is bounded by two rigid carbon planes: the right one is attached to the CNT to avoid colliding with the reservoir, and the left one is movable to mimic a piston for being impacted by a foreign object. The impactor is also modeled by a rigid mass and it collides the reservoir with a given initial velocity (energy), generating a pressure wave traveling from left to right – if P_w exceeds P_i, water infiltration would occur. The receiver is a rigid carbon plane and fixed in space throughout simulations. Its physical separation with the CNT will help extracting the transmitted force with high resolution and sensitivity through their fore interaction. Afterwards, the system may bounce back (and the impactor may detach from the reservoir). The force history transmitted to the receiver is recorded throughout the process, from which the transmitted impulse characteristics are obtained. Periodical boundary condition is imposed on the four lateral planes of the computational cell, mimicking an array of nanopores like that in a nanoporous material (Fig. 1). For comparison, a reference system is also setup with almost identical characteristics, except that the left end of CNT is closed and water infiltration cannot occur.

The 12–6 Lennard–Jones (L–J) empirical force field and a Coulomb potential is used to describe the intermolecular potential between atoms: $U(r_{ij})=4\varepsilon[(\sigma/r_{ij})^{12}-(\sigma/r_{ij})^{6}]+q_iq_j/4\pi\varepsilon_0r_{ij}$, where r_{ij} denotes the distance between atom i and j, σ and $\varepsilon$are the energy and length parameters, respectively. q_i and q_j are the partial charge assigned to atom i and j, respectively, and ε_0 is the dielectric constant. The PPPM (Particle–Particle Particle–mesh) technique with a root mean square accuracy of 10^{-4} is employed to handle the long range Coulomb interactions among water molecules. The L–J interactions are truncated at a cutoff distance of 10 Å suggested by Andrea et al. (Andrea et al., 1984). The water model is the rigid

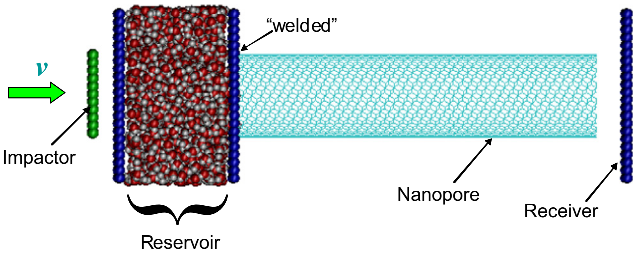

Fig. 2. The MD computational cell. This cell consists of an impactor, piston, water reservoir, boundary plane of reservoir, nanopore, and receiver (from left to right). The impactor is rigid to mimic a foreign impact loading or shocks parallel with the axial direction of the nanopore with a velocity of v; the movable piston is modeled by a rigid plane; the left open-end of the nanopore is inserted into the reservoir and is tied with the right rigid boundary plane of the reservoir; its right is closed by a rigid carbon plane. The receiver is fixed throughout MD simulation and is used to extract the transmitted force through the nanopore/water system. Periodical boundary condition is imposed to the four lateral planes of the cell.

extended simple point charge model (SPC/E) (Berendsen et al., 1987). The CNT is assumed to be rigid since its flexibility has a minor influence on the water infiltration process (Xu et al., 2011b; Zhao et al., 2009a), and that could also simulate a real “stiff” nanoporous material whose nanopore wall can effectively block lateral energy transmission. The carbon–water interaction is described by the L–J potential between carbon and oxygen atoms, with relevant parameters ($\sigma_{c-o} = 0.319$ nm and $r_{c-o} = 0.3135\ \text{kcal/mol}$) obtained from the experimental low-coverage isotherm data of oxygen adsorption on graphite which ensures the hydrophobicity of CNT (Werder et al., 2001, 2003).

Molecular dynamics (MD) program LAMMPS (large-scale atomic/molecular massively parallel simulator) is employed to carry out the numerical simulations (Plimpton, 1995). After initialization, the system is equilibrated for 100 ps to minimize system energy with NVT ensemble at ambient condition and the Nose/Hoover thermostat is used to maintain temperature with a time constant of 0.5 ps. At this moment, the water molecules are outside the CNT due to hydrophobicity. During the subsequent impact process, the NVE ensemble is employed and the history of the transmitted force, F, as well as the number of intercalated water molecules, are obtained every 2.5 ps (the simulation time step is 0.5 fs).

3.2. Fundamental behavior of CNT/water system under impact loading

Taking a representative system, which consists of a (16,16) CNT and its opening is immersed in a reservoir with 1568 water molecules, we first investigate the system response under an impacting velocity of 50 m/s (impacting energy of 9.3 fJ). The snap shots from MD simulations are given in Fig. 3. Right after the impact, the system (CNT and reservoir) starts to move toward the receiver, and the pressure in the reservoir builds up simultaneously. When the pressure wave arrives at the entrance of nanopore, the capillary resistance (its variation with impacting rate is very small (Chen et al., 2008; Zhao et al., 2009a) and not considered here) is overcome, and the highly compressed water molecules begin to invade the CNT and move toward the end of the CNT, weakening the impacting energy, as well as the magnitude and rate of transmitted force on the receiver. During this process, part of the incoming kinetic energy is converted to the potential energy of the intercalated water molecules. Owing to the confinement of the wall and pushing of the pressure wave, the infiltrated water molecules retain the highly compressed form until the pore is filled up. After the impactor bounces back, the pressure inside the water reservoir is reduced, and the transmitted force, F, begins to decrease; meanwhile, the confined water molecules recede due to the non-wetting surface of CNT, making the system fully reusable for repeated impact/blast loading. We should note that the choice of force field between the receiver and CNT will affect the magnitude of transmitted force and since our focus is on its comparison with that through the reference system so that the mechanism of energy dissipation can be elucidated easily, rather than on a single transmitted force through the nanopore/liquid system, the most popular L–J potential is thus employed to characterize their interaction (i.e., Van der Waals force).

Fig. 4 (a) gives the history of the transmitted force, which increases with infiltration, and it peaks at almost the same time when the CNT is filled with compacted water molecules, and then it decreases at a slower rate upon unloading. Comparing with the reference system, in the NEC system the peak load arrives later and the overall impulse time is longer, and the force reduction is prominent. In what follows, we explore the fundamental mechanism of energy capture through the characteristics of intercalated water molecules.

3.3. Characteristics of NEC: effect of impact velocity (v)

3.3.1. Reduction of transmitted force and impulse energy

For the same the CNT/water system employed above, Fig. 4(a) and (b) present the transmitted force under $v = 50$ m/s with impacting energy of 9.3 fJ and 30 m/s with impacting energy of 3.35 fJ, respectively. We define the dimensionless reduction of the peak transmitted force as $\Delta F = (F_{\max} - {F_{\max}}')/{F_{\max}}' \times 100\%$, where $F_{\max}$ and $F'_{\max}$ are the maximum transmitted force in the NEC system and reference system, respectively. The calculated ΔF is 67.8% and 67.6% for $v = 30$ m/s and 50 m/s, respectively. Fig. 5(a) further plots ΔF as a function of v and their associated impacting energy, E_{input}, where for the present CNT geometry, ΔF varies nonlinearly and arrives maximum at the velocity of about 40 m/s.

The total transmitted impulse energy (on the receiver) can be estimated as $W = \xi \int_0^t F^2 dt$ (Lu and Yu, 2003), which is integrated over the entire impulse duration (see below), where ξ is material parameters and can be deemed the same for NEC and reference systems. Similarly, a dimensionless reduction of the transmitted impulse energy is defined as $\Delta W = (W - W')/W' \times 100\%$ with respect to the reference system. Fig. 5(a) shows that ΔW has a similar nonlinear trend like that of ΔF, and reaches the maximum at about $v = 30$ m/s for the current CNT geometry. Both the maximum ΔF and ΔW depend on the nanopore size, whose details are given below.

3.3.2. Elongation of impulse duration

Another parameter of interest is the total time of the transmitted impulse. With respect to Fig. 4, we define the dimensionless ratio between the total transmitted impulse duration of the NEC system (τ_{NEC}) and reference system (τ_{Ref}) as $\bar{\tau}$. The dash curve in Fig. 6(a) shows that $\bar{\tau}$ reaches maximum at about $v = 30$ m/s for the current CNT geometry, consistent with the maximum impulse energy reduction (dash curve in Fig. 5(a)), and implies the best performance of energy mitigation.

The increased duration of transmitted impulse is directly related to the infiltration and defiltration processes of water molecules. The number of water molecules inside the CNT is examined and plotted in Fig. 6(b). It can be seen that the

Time (ps)	H_2O # inside CNT	Top view	Side view
0	0	-	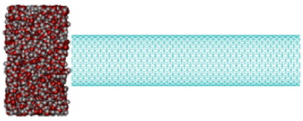
45	304	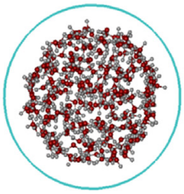	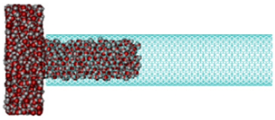
58.75	693	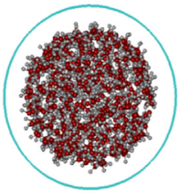	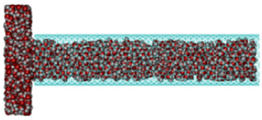
87.5	1013	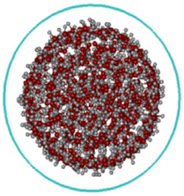	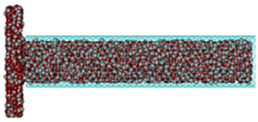
145	689	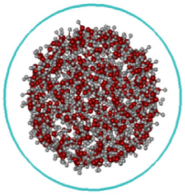	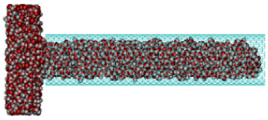
265	309	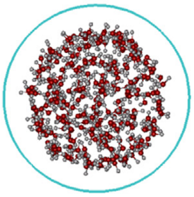	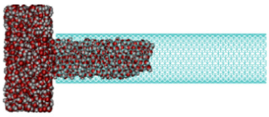
348.75	1	-	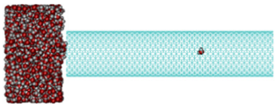

Fig. 3. Snapshots of water molecules invading and receding from the (16,16) CNT. All water molecules are included in side views; while only water molecules inside the CNT are given in top views, and indicate the layered-structure of intercalated molecules. The diameter (D) and length (L_0) of the CNT are 2.17 nm and 9.84 nm, respectively; the impacting velocity (v) is 50 m/s(impacting energy of 9.3 fJ). The right blue line represents the receiver position and the color "blue" is just consistent with "blue atoms" of the receiver in MD model. (For interpretation of the references to color in this figure legend, the reader is referred to the web version of this article.)

infiltration process is rather quick, whereas the defiltration is much slower. The rates of infiltration and defiltration are also consistent with the impact velocity (despite that more water molecules invade the CNT at higher speed). The faster defiltration rate occurring at higher v is likely caused by the larger potential energy captured inside the hydrophobic CNT. According to Fig. 6(b), another dimensionless parameter, τ_{de}/τ_{in}, can be defined as the ratio between the defiltration and infiltration times of water molecules. Fig. 6(a) shows that τ_{de}/τ_{in} increases with v, that is, for higher speed/energy impact, defiltration is relatively more difficult due to the resistance of potential energy of water molecules left in the reservoir.

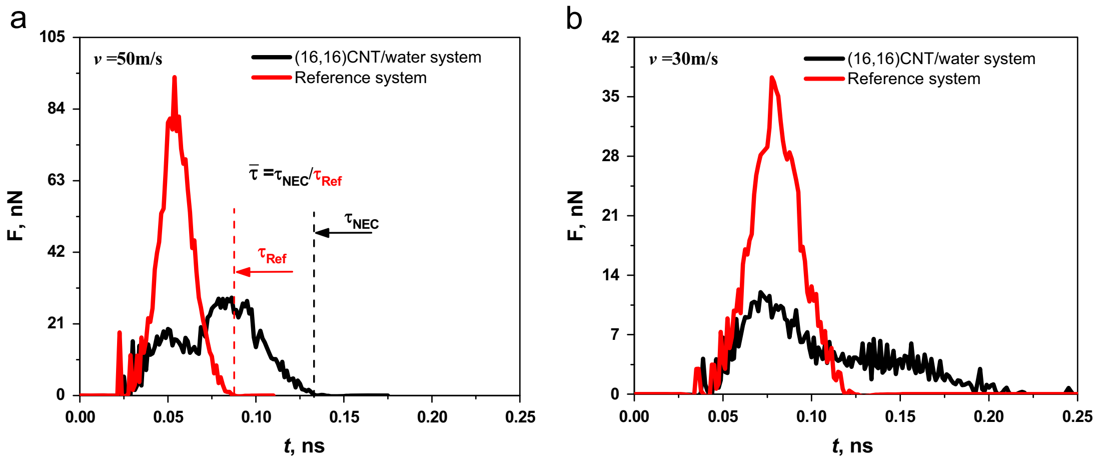

Fig. 4. The history of transmitted force under impacting velocity of (a) $v=50$ m/s and (b) $v=30$ m/s. The CNT size $D=2.17$ nm, $L_0=9.84$ nm. $\bar{\tau}$ is the ratio of impacting duration on the nanofluidic energy capture system (τ_{NEC}) to the reference system(τ_{Ref}).

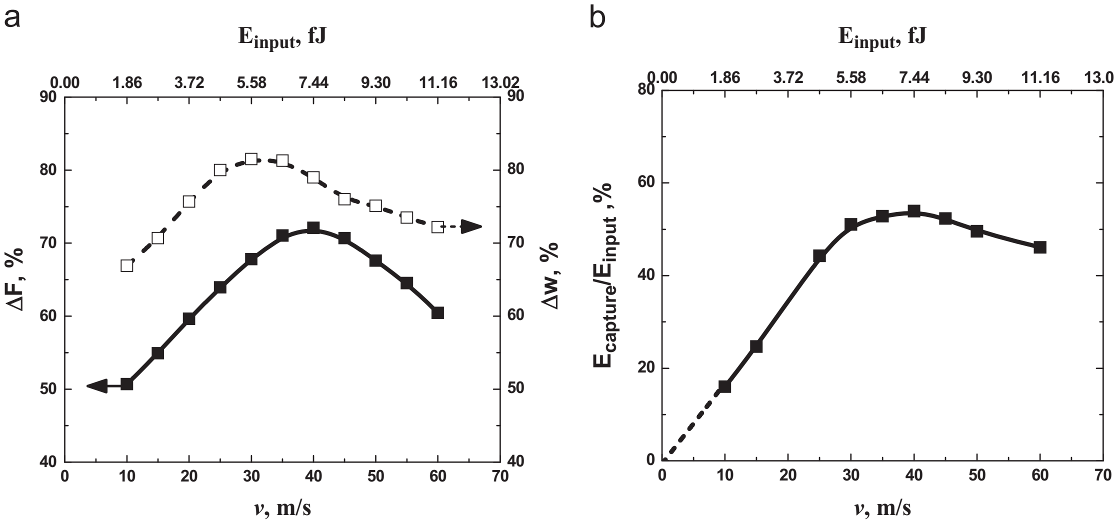

Fig. 5. (a) The reduction of the peak transmitted force, ΔF, and the total energy mitigation, ΔW, in comparison to the reference counterpart upon impact loading; (b) The ratio between the captured energy of the intercalated water molecules and the total incident/impact energy, $E_{capture}/E_{input}$, under different impacting velocities. The CNT size $D=2.17$ nm, $L_0=9.84$ nm.

3.3.3. Captured energy

To estimate the captured energy, we calculate the ratio between the variation of potential energy of the intercalated molecules with respect to that of bulk configuration, and calculated at the instant of the peak transmitted force and the incoming kinetic energy, $E_{capture}/E_{input}$. Fig. 5(b) shows that $E_{capture}/E_{input}$ increases with v when v is relatively low, and it reaches a peak value (as much as 60% for the present CNT geometry) at about 40 m/s and then slowly reduces with further increase of v. Indeed, when the impact speed is low the intercalation process is less prominent and the CNT may not even be filled, and thus less energy is mitigated. With the increases of v, more water molecules and their associated potential energy are captured; moreover, the reordering of confined water molecules in nanopores may further increase the capacity of NEC, discussed later. Nevertheless, the maximum potential energy of water molecules that may get captured in the nanopore depends on both pore geometry and impact speed. If v is very high, although the confined molecules can be more compacted (and $E_{capture}$ is higher), however the incoming kinetic energy is even higher; thus, $E_{capture}/E_{input}$ becomes smaller. When the curve in Fig. 5(b) is extrapolated to $v=0$ m/s, there is no infiltration and no energy capture.

Note that from an energy point of view, when non-wetting liquids are forced to infiltrate a nanopore, part of the external work converts to the excessive solid–liquid interfacial tension, and there is also energy dissipation through the friction resistance exacted to the liquid by solid atoms when the infiltrated liquid segment transports in the nanopore, especially for rough tubes like silica nanotube (Surani et al., 2005). For the CNT employed in the present paper, due to the weak hydrophobicity and nearly frictionless surface of CNT (Supple and Quirke, 2003; Whitby and Quirke, 2007), the contributions of both terms are much smaller than $E_{capture}$, which is a distinctive characteristic of the NEC mechanism.

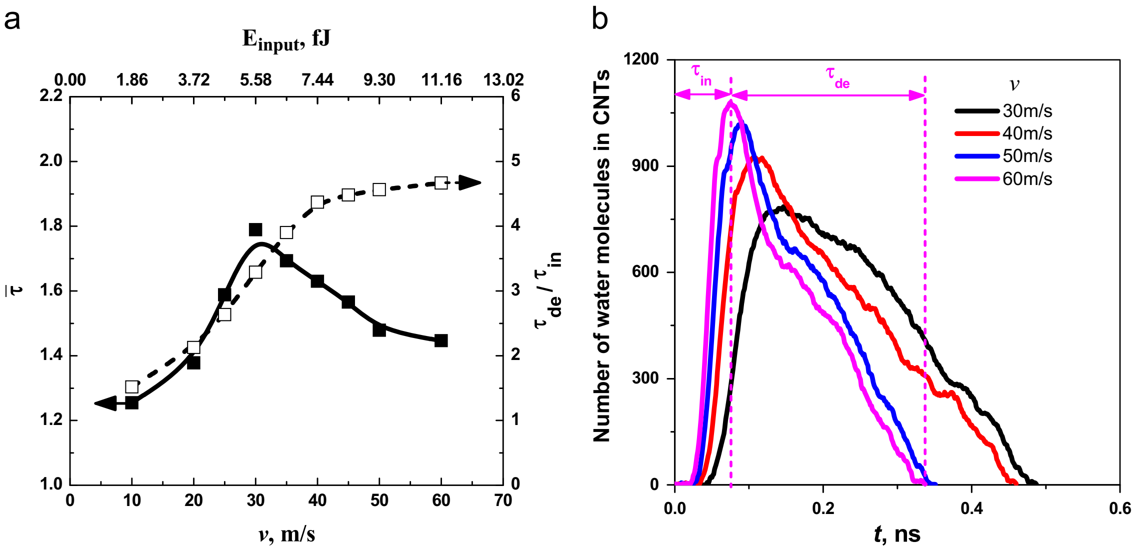

Fig. 6. (a) The ratio of impacting duration on the NEC system to the reference system, $\bar{\tau}$, and the ratio of defiltration time to infiltration time, τ_{de}/τ_{in} and (b) number of water molecules in the CNT under different impacting velocity. The CNT size D=2.17 nm, L_0=9.84 nm.

3.4. Characteristics of NEC: effect of nanopore length (L_0)

The nanopore volume is an important parameter determining the capacity of captured wave energy. The longer CNT is, the more water molecules may intercalate, the larger reduction of the transmitted force and impulse energy, and the longer invasion time leads to longer duration of the transmitted impulse. Once the CNT is filled, unless the ordering of confined water molecules is adjusted, it becomes somewhat difficult to accommodate more water molecules; even if reconfiguration is possible, the room for intercalating more liquid phase is limited within the nanoconfinement.

Consider a representative (16,16) CNT/water system under an impact velocity of 50 m/s, and L_0 varies from 4.92 nm to 11.7 nm. Fig. 7 shows the transmitted force history for nanopore length L_0=4.92, and compared with a larger L_0=9.84 (Fig. 4 (a)), apparently both the transmitted force reduction and impulse elongation are more prominent with the longer nanochannel. In Fig. 8(a), both the reduction of the transmitted peak force, ΔF, and reduction of the transmitted impulse energy, ΔW, increase with CNT length. For the same impacting energy, the pressure wave generated in the reservoir is the same, and thus the intercalated water molecules carry approximately the potential energy per molecule. This explains the essentially linear variation of $E_{capture}/E_{input}$ with L_0 in Fig. 8(b), as well as the trend of ΔW and ΔFin the dash curve Fig. 8(a), within the current space of parameters under study. Fig. 9(a) indicates that the dimensionless impulse time, $\bar{\tau}$, also increases monotonically with CNT length, which is associated with the time required to enter and exit the tube.

From the histories of confined water molecules in Fig. 9(b), the infiltration rate is the same owing to the same impact velocity/energy. Likewise, the defiltration rates are close due to the similar level of compression of confined water molecules; however, when the nanopore gets very long there are fewer water molecules remaining in the reservoir when the pore is filled and when defiltration gets started, which imposes less resistance to defiltration, leading to a relatively faster outflow. These observations are consistent with the plot of τ_{de}/τ_{in} in Fig. 9(a). Note that in this section, the initial reservoir volume is fixed. On the other hand, if the initial reservoir volume increases proportionally with pore volume as the pore length is increased, then the infiltration and defiltration rates will be essentially independent of pore length.

3.5. Characteristics of NEC: effect of nanopore diameter (D)

In this section, as we vary the diameter of CNT (with its length fixed at 9.84 nm), the length of reservoir is regulated so as to keep the same volume ratio between CNT and reservoir. This approach may help to reveal the pore size effect more clearly. The number of initial water molecules in reservoir is adjusted accordingly so as to keep the density of water inside the reservoir close to that of bulk water, ρ_0=998.0 kg/m^3 at 1 atm and 300 K after equilibrium. The impact velocity is fixed at 50 m/s with impacting energy of 9.3 fJ.

Fig. 10 shows the history of the transmitted force for D=1.35 nm ((10,10) CNT). Compared with a larger nanopore diameter, D=2.17 nm ((16,16) CNT) shown in Fig. 4(a), with the increase of CNT diameter, more kinetic energy will be captured, leading to the reduction of the transmitted force and impulse energy, and the elongation of impulse duration. Fig. 11 (a) gives the quantitative results of ΔF and ΔW as a function of D, where a nonlinear increasing trend is observed, and also similar for $E_{capture}/E_{input}$ in Fig. 11 (b). The nonlinear variation is related to the lateral diffusion effect that is more prominent in larger CNT. Note that with the increment of D, although more energy gets captured, the energy capture per

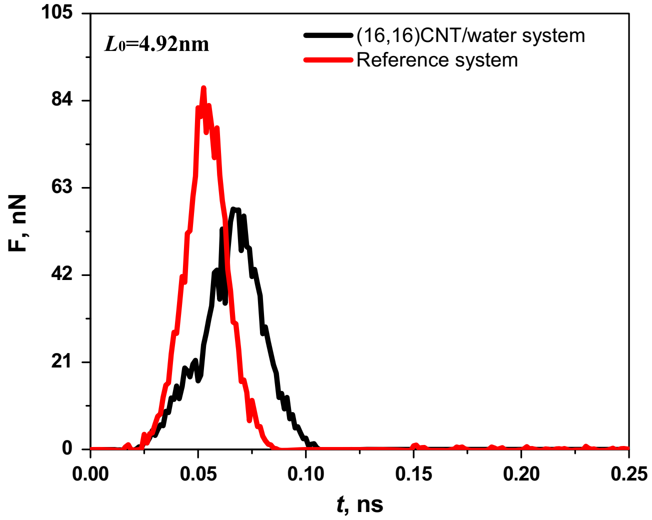

Fig. 7. The history of the transmitted force measured in (16,16) CNTs/water system with the length of the CNTs (L_0) of $L_0=4.92$ nm. The diameter of the CNTs, $D=2.17$ nm, and impacting velocity, $v=50$ m/s.

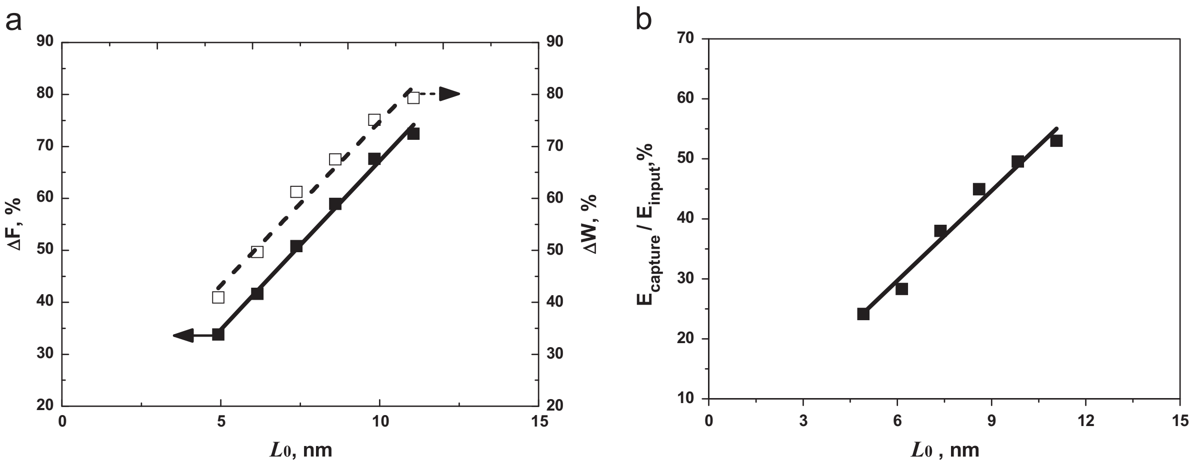

Fig. 8. (a) The reduction of the peak transmitted force, ΔF, and the total energy mitigation, ΔW; and (b) The ratio between the captured energy of the intercalated water molecules and the total impact energy, $E_{capture}/E_{input}$ with different lengths of CNTs. The diameter of the CNTs, $D=2.17$ nm, and impacting velocity, $v=50$ m/s.

unit volume does not necessary increase, which will be discussed later. The dash curve in Fig. 12(a) confirms that the dimensionless transmitted impulse time increases with CNT diameter.

Fig. 12(b) presents the variation of the number of intercalated water molecules. Since the infiltration pressure (capillary resistance) is smaller at larger D (Falk et al., 2010; Pascal et al., 2011; Xu et al., 2011b), a higher infiltration rate is obtained. In a larger CNT, the initial defiltration rate is higher owing to the more prominent release of the captured energy, but later the defiltration becomes slower since more molecules need to be evacuated. Overall, τ_{de}/τ_{in} increases with the increase of D.

3.6. Underlying molecular mechanism

As illustrated in Fig. 1, once the potential energy-carrying water molecules invade into the nanopore, they may rearrange their configurations (in particular under higher speed impact) owing to the carbon–water interfacial interaction, which may potentially affect the capacity of energy capture and impact duration. The study of the axial and radial density profiles of water molecules may reveal some insights of the molecular mechanisms.

Taking the (16,16) CNT/water system as a representative example, Fig. 13(a) gives the density profile of water molecules along the axial direction of CNT under the impact velocity of 30 m/s. During the infiltration stage, the water density is fairly high near the entrance of the CNT, owing to the pressure wave that overcomes the capillary resistance and that keeps feeding water into the CNT. On the other hand, for water molecules that have invaded the CNT, the axial density is approximately a constant (along the axial direction) and much higher than that of bulk water – this suggests that the

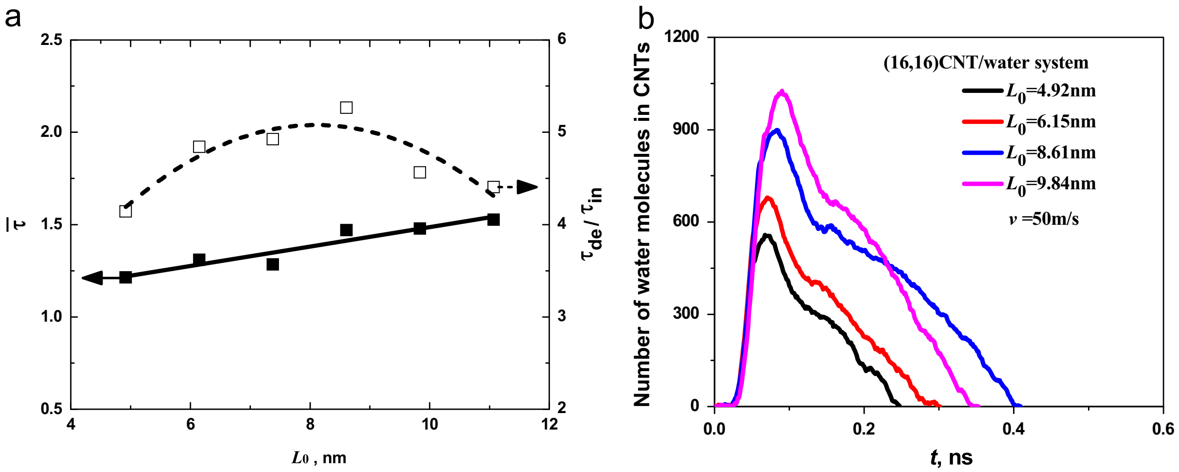

Fig. 9. (a) The variation of $\bar{\tau}$ and τ_{de}/τ_{in} with the CNT length, and (b) number of water molecules inside (16,16) CNTs with different lengths. The diameter of the CNTs, $D=2.17$ nm, and impacting velocity, $v=50$ m/s.

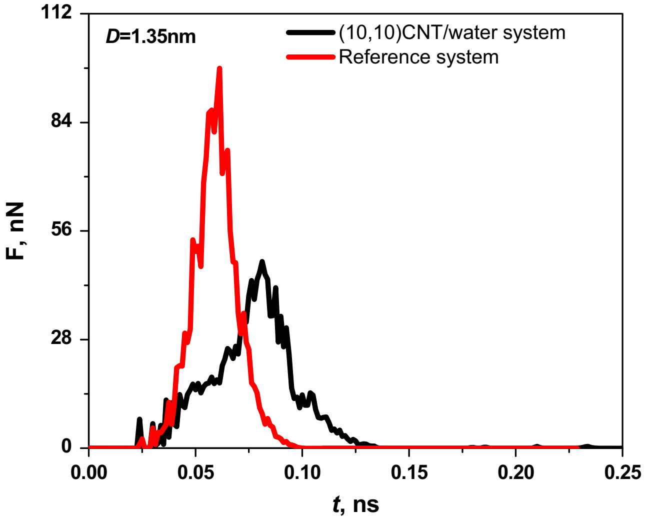

Fig. 10. The history of the transmitted force measured from the CNTs/water system with diameter of CNTs of $D=1.35$ nm, (10,10) CNT. The CNTs size $L_0=9.84$ nm and the impacting velocity $v=50$ m/s.

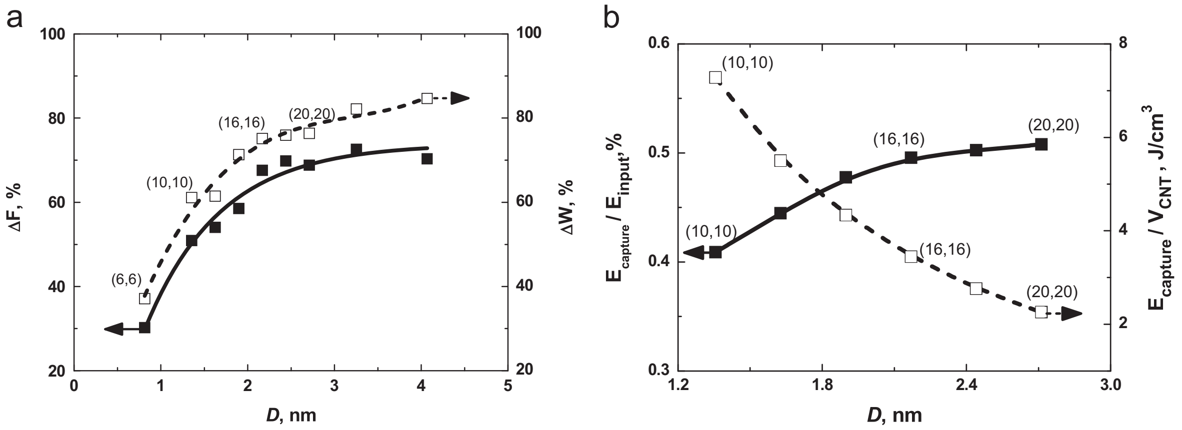

Fig. 11. (a) Variation of the peak transmitted force, ΔF, and total energy reduction, ΔW, with different diameters of CNTs. The length of CNTs is 9.84 nm and the impacting velocity is 50 m/s; (b) The ratio between the captured energy of the intercalated water molecules and the total impact energy, $E_{capture}/E_{input}$. The CNTs size $L_0=9.84$ nm and the impacting velocity $v=50$ m/s.

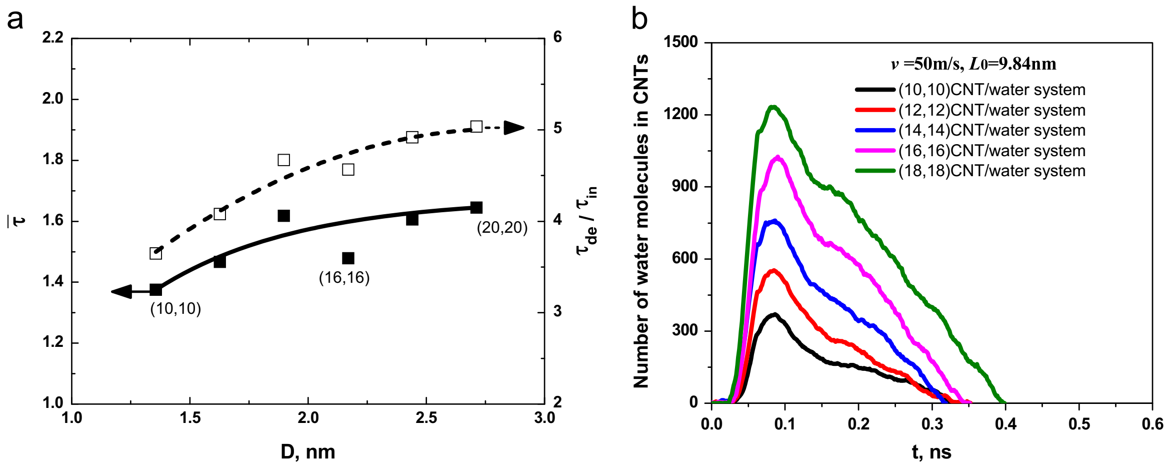

Fig. 12. (a) The variation of $\bar{\tau}$ and τ_{de}/τ_{in} with the diameter of CNTs, and (b) Number of water molecules in CNTs with different diameters. The CNTs size L_0=9.84 nm and the impacting velocity v=50 m/s.

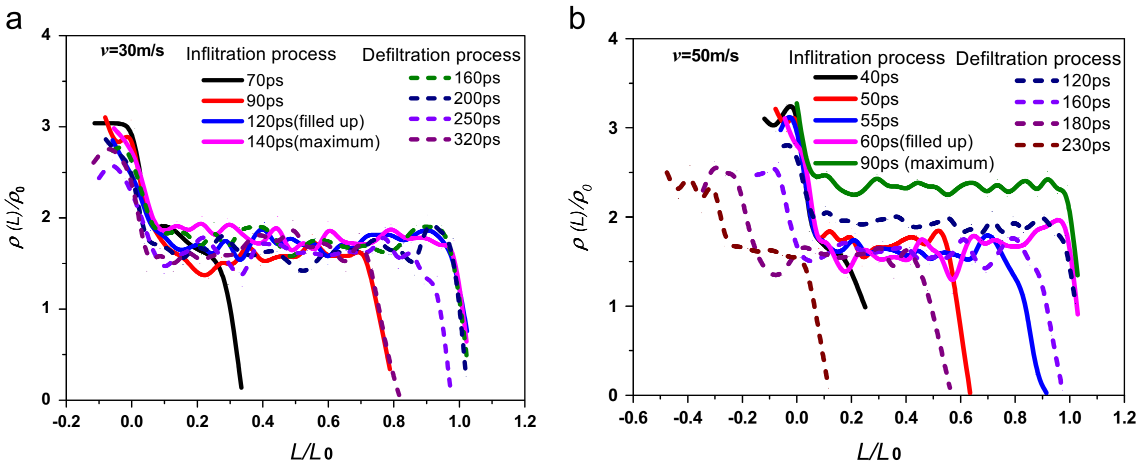

Fig. 13. Normalized density profile, $\rho(L)/\rho_0$, of water molecules along the axial direction of the CNT/water system (i.e., the impacting direction) at different moments under the impacting velocity of (a) v=30 m/s and (b) v=50 m/s. The CNT size D=2.17 nm, L_0=9.84 nm.

excessive potential energy carried by every intercalated water molecule is about the same. Structural transition of water molecules may occur in a nanoenvironment under a high pressure, like phase transformation (Bai et al., 2006; Koga et al., 2001; Srivastava et al., 2011; Takaiwa et al., 2008). However, since the most of popular water model including SPC/E model employed in the present simulation cannot give a stable and real crystal structures like ice phase using the general MD technique (Alexiadis and Kassinos, 2008), the structural evolution of highly compacted water molecules in CNTs is not focused here. The axial density is also almost the same at different instants of infiltration (as well as when the pore is filled up and during defiltration), indicating the cluster movement of compacted water molecules (Vaitheeswaran et al., 2004).

At a higher impact velocity (50 m/s), shown in Fig. 13(b), the axial density increases as the infiltration proceeds, which indicates that under stronger pressure wave and confinement of nanopores, the intercalated molecules becomes more compacted (which requires the reordering of the molecules); on the other hand due to the volumetric constraint, there is an upper limit of the maximum captured energy (and the axial density is the highest when the pore is filled up) for a given pore geometry. Likewise, the axial density decreases with defiltration (and at any instant, the density remains fairly uniform in the axial direction). In other words, the energy is captured and released through continuous “clusters” of compressed molecules, and the capture and release rates are different. In addition, the density profiles in Fig. 13 indicate that the compaction level is approximately constant along the axial direction, and thus the captured energy varies almost linearly with L_0, consistent with the findings in Fig. 8(b).

Fig. 14 gives the radial density profile of water molecules inside the CNT. A fluctuation is observed due to competition between water–water and water–carbon interactions, showing a layered model structure of water molecules at the radial direction, similar to that at equilibrium (Hummer et al., 2001; Thomas and McGaughey, 2008; Werder et al., 2001). Such a layered structure can also be seen from Fig. 3 (top view). The magnitude of the first solvation shell (FSS) becomes smaller with the increase of velocity (Joseph and Aluru, 2008; Thomas and McGaughey, 2008), implying the water molecules are

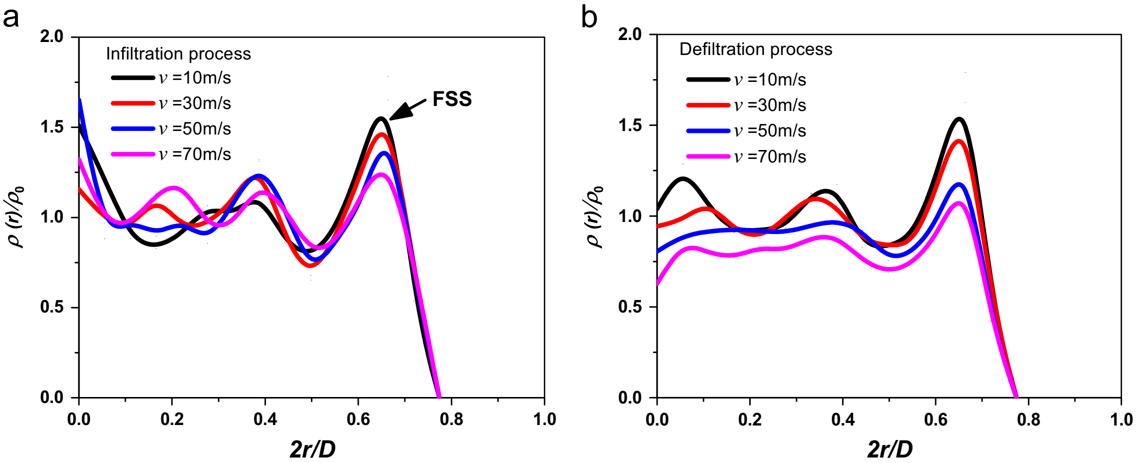

Fig. 14. Normalized average radial density profile, $\rho(r)/\rho_0$, of intercalated water molecules during the (a) infiltration process and (b) defiltration process, under different impacting velocities. The CNT size $D=2.17$ nm, $L_0=9.84$ nm.

more closely-packed with stronger pressure waves, leading to higher captured potential energy. The decreased FSS also echoes with that under high nanofluidic transport rate (Xu et al., 2012). The radial density profile upon defiltration is more uniform than that during infiltration (which is consistent with the less ordering of confined molecules during defiltration in Fig. 3), indicating a more "uniform" releasing of the captured energy.

The reduction of transmitted force and impulse energy with the increase of CNT diameter can also be understood by the ordering of intercalated water molecules. Fig. 15 gives the axial and radial density profiles of water molecules at different D. In the smaller CNT, despite fewer captured molecules, the axial density is higher, with more captured energy per volume. The result implies that higher porosity (with smaller pore size) will in general benefit the overall performance of energy mitigation.

3.7. *Extend to silica nanopores*

In order to study effect of solid–liquid interaction on NEC, the CNT is replaced with a silica nanotube (SNT) in this section. The SNT is neutral overall with the partial charge in each silicon and oxygen atom of 0.89e and -0.445e, respectively. The L–J parameters for interaction between the SNT and water molecules are $\sigma_{o'-o}=0.333$ nm, $r_{o'-o}=0.153$ kcal/mol and $\sigma_{si-o}=0.3731$nm, $r_{si-o}=0.216$ kcal/mol, where Si, O', and O represent the silicon and oxygen atoms in the SNT model, and oxygen atom in the SPC/E water model. With these parameters, the SNT also behaves a hydrophobic interaction with water molecules (Xu et al., 2011b). A larger SNT with $D=2.05$ nm and a smaller SNT with $D=0.84$ nm are investigated – their diameter are analogous to that of a (16,16) CNT and a (6,6) CNT, respectively. When the diameter of SNT is varied, the reservoir volume is regulated accordingly, like that in the study of CNT diameter effect described above. The length of all tubes is fixed at 9.8 nm in this section.

For the larger tube diameter, Fig. 16(a) shows the transmitted force history, with $\Delta F=69.09\%$ and $\Delta W=72.44\%$, and for the smaller tube in Fig. 16(b), $\Delta F=41.6\%$ and $\Delta W=45.69\%$. The trends are similar to the size effect of CNTs (see Fig. 11), where ΔF and ΔW are 67.6% and 75.1% respectively for the larger (16,16) CNT, and 42.90% and 52.75% respectively for the smaller (6,6) CNT. Thus, in the silica system the reduction of transmitted force is larger than the CNT counterpart, whereas the reduction of transmitted impulse energy is smaller. The partially charged surface of SNT results a stronger interfacial interaction with water molecules (Xu et al., 2011a), leading to fewer intercalated water molecules and thus less reduction of transmitted impulse energy. Meanwhile the stronger interfacial interaction of SNT results in a higher effective shear stress, and that could reduce the transmitted force. The differences between SNT and CNT, however, are relatively small since the NEC mechanism is more dominant.

4. Experimental verification

In order to verify the nanofluidic energy capture mechanism, an impact test on nanoporous zeolite–water liquid system was performed. The as-received material zeolite from Zeolyst was in particle form with the size of 10–30 μm. The processing and post-processing treatment procedures have been employed to obtain a slightly hydrophobic inner surface of nanopores, and discussed elsewhere (Kim et al., 2008). The after-treated nanoporous particles were compressed at 1 MPa for 1 min to form a disk-like geometry. Through a Tristar-3000 gas absorption analyzer (Gemini, The Netherlands) (Gregg and Sing, 1982), the nanoporosity was about 0.24 ml/g, the nanopore surface area was 700 m^2/g, and the average nanopore size was 7.0 nm. Besides, the nanopores were open. The nanoporous zeolite disk was put into polypropylene pad. After deionized water was added on this polypropylene pad, with its mass ratio to nanoporous particles of 1:2.5, the pad was thermally

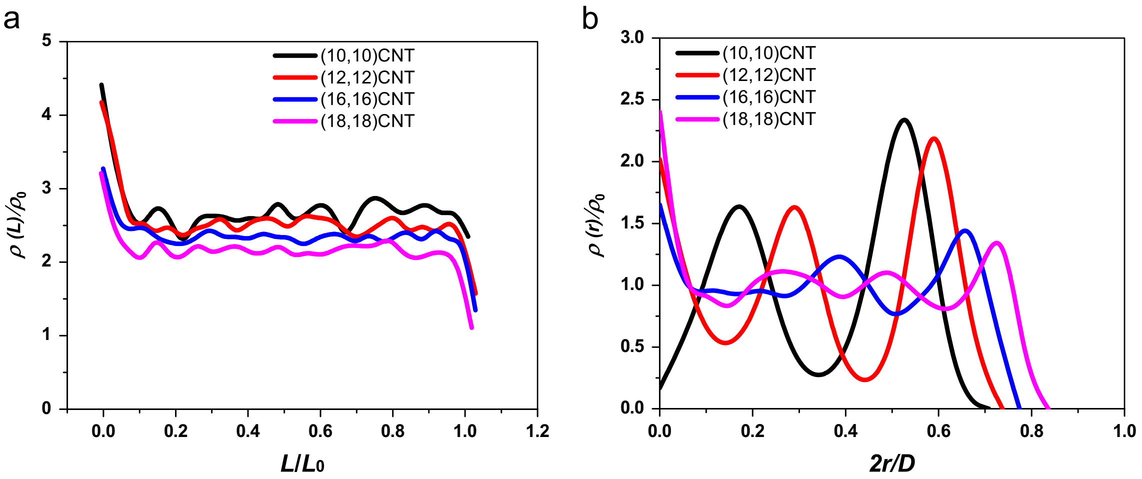

Fig. 15. (a) Normalized average density profile, $\rho(L)/\rho_0$, of water molecules along the axial direction of the CNTs/water system and (b) Normalized average radial density profile,$\rho(r)/\rho_0$, of water molecules inside CNTs at the infiltration process with different diameters of CNTs. The CNT size L_0=9.84 nm; the impacting velocity v=30 m/s.

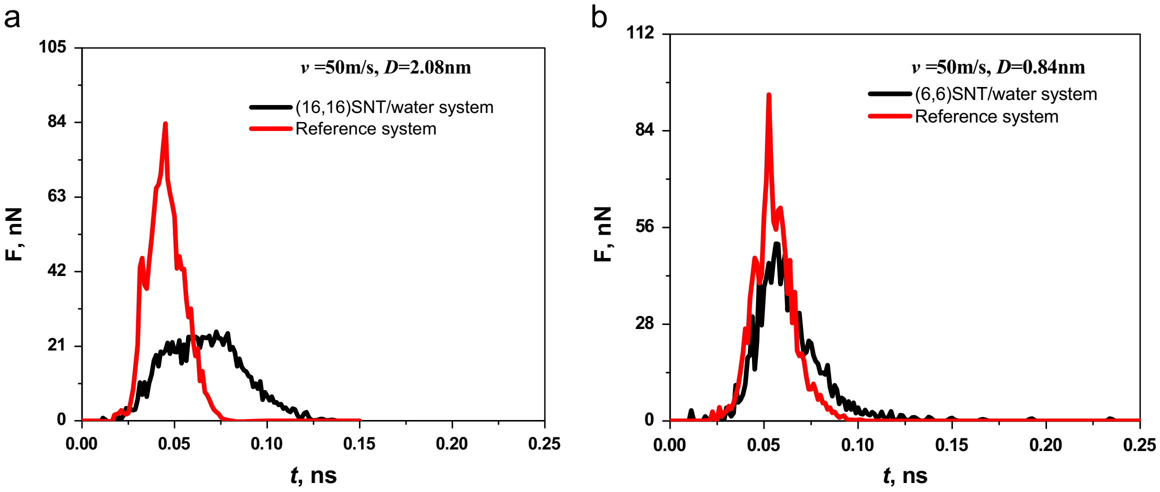

Fig. 16. Transmitted force measured from (a) (16,16) SNT/water system and (b) (6,6) SNT/water system. The impacting velocity v=50 m/s.

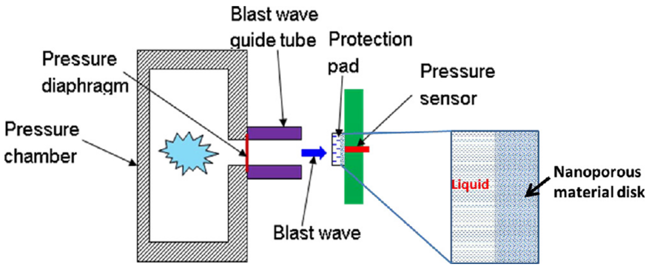

Fig. 17. The blast chamber setup. A high intensive pressure is generated in the pressure chamber, and propagates along the guide tube after breaking through the diaphragm, and then arrives at the testing sample. The testing sample is tightly attached on the green supporting platform. The transmitted force of input pulse through the sample can be collected through the red pressure sensor.

sealed for a testing sample. The overall thickness of one testing sample was 2.3 mm. By using adhesives, the sample was strongly glued to the surface of an aluminum supporting platform, and immediately behind the sample, a pressure transducer was tightly mounted inside the stage and pressed firmly against the back of the pad, as illustrated in Fig. 17.

In order to generate a high impacting wave, a blast chamber setup was designed, shown in Fig. 17. This high-pressure chamber was made of 2.54 mm thick solid aluminum alloy with cross-sectional diameter in 203 mm and depth in 254 mm.

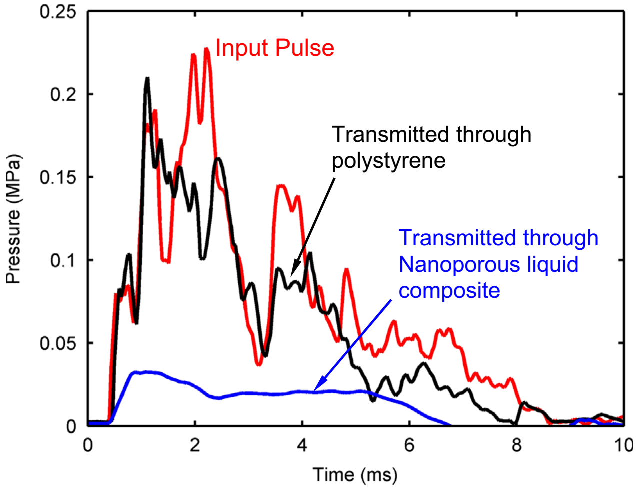

Fig. 18. Typical blast impacting pulse and measured transmitted pressure through the polystyrene (EPS) and nanopore–liquid composite samples.

A high pressure up to 1.2 MPa could be generated in the chamber by using a 1.6 hp Craftsman A13277 compressor. A vinyl diaphragm with thickness of 0.4 mm was placed at the front of the chamber to trigger a blast wave. When the generated pressure inside the chamber reached the limit of the diaphragm, the diaphragm would break up, generating a Friedlander wave. The wave would propagate through the guide tube, and impact on the testing sample which was placed about 10 cm away. The transmitted force when the impacting wave transported through the testing sample could be measured by a pressure transducer which connected with the testing sample behind. The input pulse was directly measured by a similar pressure transducer that was mounted 25.4 mm away in the mounting stage, open to the air. In addition, a testing sample of standard 6-lb expanded polystyrene (EPS) was employed for comparisons as a representative of conventional energy absorption materials (EAM).

Fig. 18 shows typical measurement results of the input and transmitted waves. When the wave propagates through the EPS sample, at the beginning stage, the profile of the wave is nearly identical with the input pulse, implying that buckling deformation of cells does not occur at such a short time (with respect to the fast input impacting wave energy), since cell buckling usually takes a few milliseconds (Bureau and Genron, 2003; Han et al., 2008). After the first 1.5 μs, the pressure reduction takes place evidently compared with generated pressure (input pulse), indicating that energy absorption happens. During the following overpressure plateau, the maximum pressure is reduced by about 20–30%.

When the wave transmits through the mixture of nanopore/liquid testing sample, the pressure reduction takes place almost immediately at onset of pressure rising, thanks to the NEC mechanism. At the overpressure stage, a much pressure reduction is observed compared with both the input and EPS curve and the peak pressure is only 0.035 MPa. The maximum reduction of transmitted pressure is about 85% and 80% of that input pulse and EPS sample, respectively, showing that the developed nanopore–liquid system can mitigate energy more efficiently and much faster. After this apparent energy and force reduction, most of the input wave energy does not reach the pressure transducer, and a small oscillation of transmitted force is observed till to completely be dissipated at 10 ms around. More importantly, the transmitted pressure curve is quite smooth including the major low-pressure valleys. As a result, the transmitted wave profile consists of only a single phase, with a slowly-rising, non-shock front, followed by a slowly-decreasing plateau, implying that part of input energy is captured by the liquids, which qualitatively verifies above MD simulations.

We note that the present comparison between simulation and experiment is rather qualitative due to the several limitations and practical challenges. For example, the pore network in zeolite is quite complicated in the experimental systems and the diameter of pores is also not quite uniform. Besides, the surface of zeolite is modified for obtaining slight hydrophobicity in experiment, making it difficult to incorporate the exact surface structure in simulation. In addition, the scale difference between simulation cell and experiment system is another factor for challenging a quantitative match between simulation and experiment. Nevertheless, the qualitative matching trends shown in simulation and experiment have demonstrated the feasibility of the current MD model, and more quantitative coordination will be carried out in future.

5. Concluding Remarks

When an intensive stress wave is acted on a non-wetting liquid–nanoporous solid composite material system, we report a new protection mechanism of nanofluidic energy capture (NEC). A significant part of the incident impact or blast wave energy can be quickly converted to the potential energy of infiltrated water molecules and is temporarily captured (until the nanopores are filled up), leading to a prominent reduction in both the transmitted force and energy (as well as elongation of the transmitted impulse duration), and the captured energy is then gradually released. The NEC system has the unique advantage of high energy mitigation density and low working pressure (ensuring safety and comfort), fast response time (on the order of ns) and it can be used repeatly; all these features making it ideal for mitigating highly intense stress waves.

MD simulations show that limited by the capacity of CNT, the maximum captured energy is a function of nanopore size, pore composition, and impacting velocity; for given pore properties, there is an optimum velocity at which the NEC mechanism is the most prominent. At a given impact velocity, the reduction of transmitted force and impulse energy increase with the increase of nanopore length and diameter, however the energy captured per volume decreases with increasing nanopore diameter. Molecular simulations show that the energy is captured and released through cluster movement of compacted water molecules. A blast experiment on a nanoporous zeolite/water system is carried out and the results qualitatively verify the MD findings.

Acknowledgment

The work is supported by National Science Foundation (CMMI-0643726 and ECCS-1028010), DARPA (W91CRB-11-C-0112), National Natural Science Foundation of China (11172231), and Changjiang Scholar Program from Ministry of Education of China.

References

Alexiadis, A., Kassinos, S., 2008. Molecular simulation of water in carbon nanotubes. Chem. Rev. 108, 5014–5034.

Andrea, T.A., Swope, W.C., Andersen, H.C., 1984. The role of long ranged forces in determining the structure and properties of liquid water. J. Chem. Phys. 79, 4576–4584.

Bai, J., Wang, J., Zeng, X.C., 2006. Multiwalled ice helixes and ice nanotubes. Proc. Natl. Acad. Sci. USA 103, 19664–19667.

Berendsen, H.J.C., Grigera, J.R., Straatsma, T.P., 1987. The missing term in effective pair potentials. J. Phys. Chem. 24, 6269–6271.

Bureau, M.N., Genron, R., 2003. Mechanical-morphology relationship of PS foam. J. Cell. Plas. 39, 353–367.

Cao, A., Dickrell, P.L., Sawyer, W.G., Ghasemi-Nejhad, M.N., Ajayan, P.M., 2005. Super-compressible foamlike carbon nanotube films. Science 310, 1307–1310.

Chen, X., Surani, F.B., Kong, X., Punyamurtula, V.K., Qiao, Y., 2006. Energy absorption performance of a steel tube enhanced by a nanoporous material functionalized liquid. Appl. Phys. Lett. 89, 241918.

Chen, X., Cao, G., Han, A., Punyamurtula, V.K., Liu, L., Culligan, P.J., Kim, T., Qiao, Y., 2008. Nanoscale Fluid transport: size and rate effects. Nano Lett. 8, 2988–2992.

Côté, F., Deshpande, V.S., Fleck, N.A., Evans, A.G., 2004. The out-of-plane compressive behavior of metallic honeycombs. Mater. Sci. Eng. A 380, 272–280.

Daraio, C., Nesterenko, V.F., Herbold, E.B., Jin, S., 2006. Energy trapping and shock disintegration in a composite granular medium. Phys. Rev. Lett. 96, 058002.

Dharmasena, K.P., Wadley, H.N.G., Xue, Z., Hutchinson, J.W., 2008. Mechanical response of metallic honeycomb sandwich panel structures to high-intensity dynamic loading. Int. J. Impact Eng. 35, 1063–1074.

Eroshenko, V., Regis, R., Soulard, M., Patarin, J., 2001. Energetics: a new field of applications for hydrophobic zeolites. J. Am. Chem. Soc. 123, 8129–8130.

Evans, A.G., Hutchinson, W., Fleck, J., Ashby, N.A., Wadley, H.N.G., M.F., 2001. The topological design of multifunctional cellular metals. Prog. Mater. Sci. 46, 309–327.

Evans, A.G., He, M.Y., Deshpande, V.S., Hutchinson, J.W., Jacobsen, A.J., Carter, W.B., 2010. Concepts for enhanced energy absorption using hollow micro-lattices. Int. J. Impact Eng. 37, 947–959.

Falk, K., Sedlmeier, F., Joly, L., Netz, R.R., Bocquet, L., 2010. Molecular origin of fast water transport in carbon nanotube membranes: superlubricity versus curvature dependent friction. Nano Lett. 10, 4067–4073.

Gibson, L.J., Ashby, M.F., 1997. Cellular Solids: Structure and Properties. Cambridge University Press, Cambridge.

Gregg, S.J., Sing, K.S.W., 1982. Adsorption, Surface Area, and Porosity, 2nd Edition Academic Press, London.

Han, A., Qiao, Y., 2006. Pressure-induced infiltration of aqueous solutions of multiple promoters in a nanoporous silica. J. Am. Chem. Soc. 128, 10348–10349.

Han, A., Punyamurthula, V.K., Lu, W., Qiaoa, Y., 2008. Deformation of a nanoporous silica under compressive loading. J. Appl. Phys. 103, 084318.

Heyden, F.H.J., v.d., Bonthuis, D.J., Stein, D., Meyer, C., Dekker, C., 2007. Power generation by pressure-driven transport of ions in nanofluidic channels. Nano Lett. 7, 1022–1025.

Holt, J.K., Park, H.G., Wang, Y.M., Stadermann, M., Artyukhin, A.B., Grigoropoulos, C.P., Noy, A., Bakajin, O., 2006. Fast mass transport through sub-2-nanometer carbon nanotubes. Science 312, 1034–1037.

Hong, J., 2005. Universal power-law decay of the impulse energy in granular protectors. Phys. Rev. Lett. 94, 108001.

Hummer, G., Rasalah, J.G., Noworyta, J.P., 2001. Water conduction through the hydrophobic channel of a carbon nanotube. Nature 414, 188–190.

Joseph, S., Aluru, N.R., 2008. Why are carbon nanotubes fast transporters of water? Nano Lett. 2, 452–458.

Kazemi-Kamyab, V., Subramaniam, K., Andreopoulos, Y., 2011. Stress transmission in porous materials impacted by shock waves. J. Appl. Phys. 109, 013523.

Kim, T., Han, A., Qiao, Y., 2008. Effects of surface-group length on liquid defiltration in a MCM-41. J. Appl. Phys. 104, 034304.

Koga, K., Gao, G.T., Tanaka, H., Zeng, X.C., 2001. Formation of ordered ice nanotubes inside carbon nanotubes. Nature 412, 802–805.

Lee, J.H., Wang, L., Kooi, S., Boyce, M.C., Thomas, E.L., 2010. Enhanced energy dissipation in periodic epoxy nanoframes. Nano Lett. 10, 2592–2597.

Lindberg, H.E., Florence, A.L., 1987. Dynamic Pulse Buckling: Theory and Experiment, 1st Edition Martinus Nijhoff, Dordrecht.

Liu, C., Li, Z., 2010. Molecular dynamics simulation of composite nanochannels as nanopumps driven by symmetric temperature gradients. Phys. Rev. Lett. 105, 174501.

Lu, G., Yu, T., 2003. Energy Absorption of Structures and Materials. CRC Press, Hong Kong.

Misra, A., Greer, J.R., Daraio, C., 2008. Strain rate effects in the mechanical response of polymer-anchored carbon nanotube foams. Adv. Mater. 20, 1–5.

Moss, W.C., King, M.J., Blackman, E.G., 2009. Skull flexure from blast waves: a mechanism for brain injury with implications for helmet design. Phys. Rev. Lett. 103, 108702.

Nemat-Nasser, S., Kang, W.J., McGee, J.D., Guo, W.G., Issac, J.B., 2007. Experimental investigation of energy absorption characteristics of component of sandwich structures. Int. J. Impact Eng. 34, 1119–1146.

Pascal, T.A., Goddard, W.A., Jung, Y., 2011. Entropy and the driving force for the filling of carbon nanotubes with water. Proc.Natl. Acad. Sci.USA 108, 11794–11798.

Plimpton, S., 1995. Fast parallel algorithms for short-range molecular dynamics. J. Comput. Phys. 117, 1–19.

Qiao, Y., Cao, G., Chen, X., 2007. Effect of gas molecules on nanofluidic behaviors. J. Am. Chem. Soc. 129, 2355–2359.

Radford, D.D., McShane, G.J., Deshpande, V.S., Fleck, N.A., 2007. Dynamic compressive response of stainless-steel square honeycombs. J. Appl. Mech. 74, 658–667.

Schaedler, T.A., Jacobsen, A.J., Torrents, A., Sorensen, A.E., Lian, J., Greer, J.R., Valdevit, L., Carter, W.B., 2011. Ultralight metallic microlattices. Science 334, 962–965.
Sparreboom, W., Vandenberg, A., Eijkel, J.C.T., 2009. Principles and applications of nanofluidic transport. Nat. Nanotechnol. 4, 713–720.
Srivastava, R., Docherty, H., Singh, J.K., Cummings, P.T., 2011. Phase transitions of water in graphite and mica pores. J. Phys. Chem. C 115, 12448–12457.
Supple, S., Quirke, N., 2003. Rapid imbibition of fluids in carbon nanotubes. Phys. Rev. Lett. 90, 214501.
Surani, F.B., Kong, X., Panchal, D.B., Qiaoa, Y., 2005. Energy absorption of a nanoporous system subjected to dynamic loadings. Appl. Phys. Lett. 87, 163111.
Takaiwa, D., Hatano, I., Koga, K., Tanaka, H., 2008. Phase diagram of water in carbon nanotubes. Proc. Natl. Acad. Sci. USA 105, 39–43.
Teo, E.H.T., Yung, W.K.P., Chua, D.H.C., Tay, B.K., 2007. A carbon nanomattress: a new nanosystem with intrinsic, tunable, damping properties. Adv. Mater. 19, 2941–2945.
Thomas, J.A., McGaughey, A.J.H., 2008. Density, distribution, and orientation of water molecules inside and outside carbon nanotubes. J. Chem. Phys. 128, 084715.
Tilbrook, M.T., Deshpande, V.S., Fleck, N.A., 2006. The impulsive response of sandwich beams: Analytical and numerical investigation of regimes of behaviour. J. Mech. Phys. Solids 54, 2242–2280.
Vaitheeswaran, S., Yin, H., Rasaiah, J.C., Humme, G., 2004. Water clusters in nonpolar cavities. Proc. Natl. Acad. Sci. USA 101, 17002–17005.
Werder, T., Walther, J.H., Jaffe, R.L., Halicioglu, T., Noca, F., Koumoutsakos, P., 2001. Molecular dynamics simulation of contact angles of water droplets in carbon nanotubes. Nano Lett. 1, 697–702.
Werder, T., Walther, J.H., Jaffe, R.L., Halicioglu, T., Koumoutsakos, P., 2003. On the water–carbon interaction for use in molecular dynamics simulations of graphite and carbon nanotubes. J. Phys. Chem. B 107, 1345–1352.
Whitby, M., Quirke, N., 2007. Fluid flow in carbon nanotubes and nanopipes. Nat. Nanotechnol. 2, 87–94.
Xu, B., Chen, X., 2013. Electrical-driven transport of endohedral fullerene encapsulating a single water molecule. Phys. Rev. Lett. 110, 156103.
Xu, B., Qiao, Y., Li, Y., Zhou, Q., Chen, X., 2011a. An electroactuation system based on nanofluids. Appl. Phys. Lett. 98, 221909.
Xu, B., Qiao, Y., Park, T., Tak, M., Zhou, Q., Chen, X., 2011b. A conceptual thermal actuation system driven by interface tension of nanofluids. Energy Environ. Sci. 4, 3632–3639.
Xu, B., Kim, T., Qiao, Y., Zhou, Q., Chen, X., 2012. Temperature dependence of fluid transport in nanopores. J.Chem. Phys.
Xue, Z., Hutchinson, J.W., 2004. A comparative study of impulse-resistant metal sandwich plates. Int. J. Impact Eng. 30, 1283–1305.
Zhao, J., Liu, L., Culligan, P.J., Chen, X., 2009a. Thermal effect on the dynamic infiltration of water into single-walled carbon nanotubes. Phys. Rev. E 80, 061206.
Zhao, J.B., Culligan, P.J., Germain, J.T., Chen, X., 2009b. Experimental study on energy dissipation of electrolytes in nanopores. Langmuir 25, 12687–12696.
Zhu, H.X., Mills, N.J., Knott, J.F., 1997. Analysis of the high strainnext term compression of open-cell foams. J. Mech. Phys. Solids 45, 1875–1899.